Evaluation of Space Radiation Effects on HgCdTe Avalanche Photodiode Arrays for Lidar Applications

Xiaoli Sun*[a], James B. Abshire,[a] Jean-Marie Laurnstein,[a]
William Sullivan III,[b] Jeff Beck,[b] and John E. Hubbs,[c]

[a]NASA Goddard Space Flight Center, Codes 698, 690, and 561, Greenbelt MD 20771 USA;
[b]Leonardo DRS Electro-Optical Infrared Systems, Dallas, TX 75374 USA;
[c]Ball Aerospace & Technologies Corp./Air Force Research Lab., Albuquerque, NM 87185 USA

ABSTRACT

We report the results from proton and gamma ray radiation testing of HgCdTe avalanche photodiode (APD) arrays developed by Leonardo DRS for space lidar detectors. We tested these devices with both ~60 MeV protons and gamma rays, with and without the read out integrated circuit (ROIC). We also measured the transient responses with the device fully powered and with the APD gain from unity to >1000. The detectors produced a large current impulse in response to each proton hit but the response completely recovered within 1 μs. The devices started to have persistent damage at a proton fluence of 7e10 protons/cm^2, equivalent to 10 krad(Si) total ionization dose. The dark current became much higher after the device was warmed to room temperature and cooled to 80K again, but it completely annealed after baking at 85°C for several hours. These results showed the HgCdTe APD arrays are suitable for use in space lidar for typical Earth orbiting and planetary missions provided that provisions are made to heat the detector chip to 85°C for several hours after radiation damage becomes evident that system performance is impacted.

Keywords: infrared detectors, HgCdTe avalanche photodiodes, lidar, radiation damage

1. INTRODUCTION

HgCdTe photodiode arrays are among the most sensitive detectors in the near to mid infrared wavelengths. They have been successfully used in the Hubble Space Telescope and are part of the James Webb Space Telescope (JWST).[1-3] Single photon sensitive HgCdTe avalanche photodiode (APD) arrays with nanoseconds response times have recently been developed as detectors in lidar receivers.[4-11] NASA Goddard Space Flight Center (GSFC) has been working with Leonardo DRS Electro-Optical Infrared Systems to develop HgCeTe APD arrays for space lidar recevivers, in work supported by by the NASA Earth Science Technology Office (ESTO). DRS has successfully produced two types of HgCdTe APD focal plane arrays (FPA), a 4x4 pixel HgCdTe APD array for trace gas lidar measurements[12,13] and a 2x8 pixel linear mode photon counting (LMPC) HgCdTe APD array for swath mapping of surface elevation and atmospheric backscatter measurements.[14,15] These new lidar detectors have nearly photon sensitivity and a >90% quantum efficiency from 0.9 to 4.3 μm, which enables new classes of airborne and space-based lidar for Earth and planetary science investigations, not only for range measurements but also for spectroscopic absorption measurements.

In order to use these HgCdTe APD arrays in space, the potential for radiation damage from the space environment must be assessed. HgCdTe photodiode arrays have been tested for radiation damage and showed little impact from radiation damage expected for the JWST mission.[16-23] The only degradation found was a slight decrease in the responsivity and a slight increase in dark current. HgCdTe APD arrays are relative new and no data on the radiation damage are available at present. We have conducted series of radiation tests on the HgCdTe APD arrays by DRS. Here, we will give a brief description of the HgCdTe APD arrays by DRS, the radiation exposure test setup, and the results. We will also give an estimate of the radiation damage of these devices in a typical Earth orbiting space environment and present an annealing technique that can be performed in orbit to mitigate the effects.

*xiaoli.sun-1@nasa.gov; phone 1 (301) 614-6732

2. HGCDTE APD ARRAYS BEING TESTED

The HgCdTe APD arrays tested were developed by DRS using their high-density vertically-integrated-photodiode (HDVIP®) technology. Its architecture is shown in Fig. 1. Each APD element was a p-around-n cylindrical photodiode formed around small via in the HgCdTe film on the silicon substrate.[4-6] Each pixel consisted of four photodiodes connected in parallel. The same pixel structure was replicated into a either a 4x4 or a 2x8 pixel array. The devices had a cut-off wavelength of 4.3 μm and a quantum efficiency of >90% from 0.9 μm to the cut-off wavelength. The HgCdTe material used in both the 4x4 and 2x8 pixel devices were from the same growth process. We tested both types of the devices. The results from the 4x4 pixel devices should apply to the 2x8 pixel devices, and vice versa. Note that the HgCdTe APDs by DRS had a different device structure than other type of HgCdTe APDs by other groups.[7-11] The results from our tests may not be directly applicable to other type HgCdTe APDs.

The 4x4 pixel devices used a fanout array design in which the HgCdTe APD array was mounted on top of a silicon substrate and signals from each pixel were brought out to bond pads on the side. The HgCdTe APD array on the substrate and a siliocon read-out integrated circuit (ROIC) were mounted in close proximity on a ceramic chip carrier.[12-13] The APD outputs were wire-bonded to the ROIC input. This approach had the advantage of independent APD array and ROIC development processes and flexibility in the integration and test of the two. For example, we could bypass the ROIC and directly measure the APD array outputs in radiation damage testing. The pixels were 80x80 μm in size on an 80 μm pitch. The array was surrounded by a perimeter guard ring that consisted of identical pixels biased to the same voltage but with the output terminals (cathodes of the diodes) grounded. The electrical bandwidth of the 4x4 pixel device was 7 MHz, which was designed to optimize the signal to noise ratio (SNR) for our CO_2 lidar with 1 μs wide laser pulses.

The 2x8 pixel array design was a higher bandwidth design whereby the pixels were vertically integrated with short interconnects to preamp inputs directly beneath the pixels.[14-15] Because of the lower input stray capacitance of this design, the electrical bandwidth was much higher the noise was lower. The pixel size was 64x64 μm on a 64 μm pitch. There was also a guard ring made of the same pixels like the other devices. The devices could detect single photon events and be used in linear mode photon counting applications.

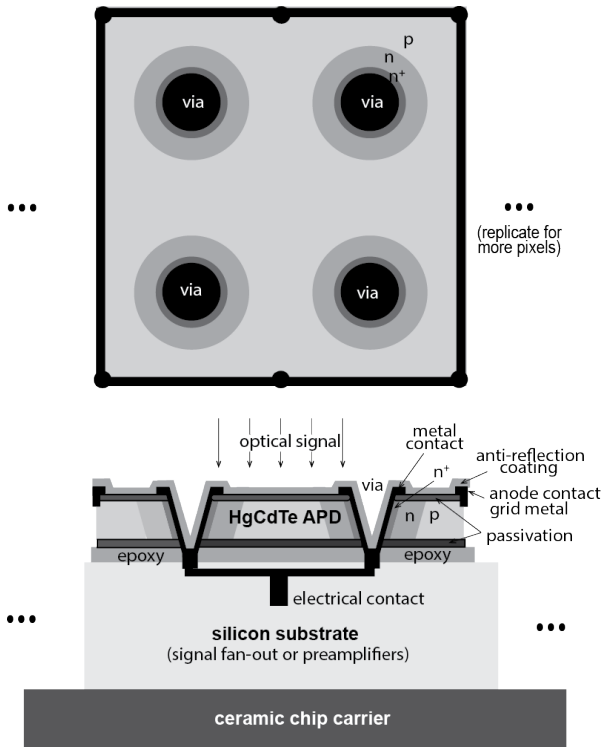

Figure 1. Schematic of the HDVIP® HgCdTe APD arrays by the Leonardo Electro-Optical Infrared Systems.

3. PROTON IRRADIATION OF 4X4 PIXEL HGCDTE APD ARRAY WITHOUT ROIC

3.1 Test setup

The proton radiation damage tests were first performed on a bare 4x4 pixel HgCdTe APD fanout array without ROIC. The tests were conducted by personnel from the Infrared Radiation Effects Laboratory (IRREL), Air Force Research Lab (AFRL) at the Crocker Nuclear Laboratory (CNL), University of California, Davis, CA, on 28-29 November 2012. The HgCdTe APD array was housed in a low background noise liquid nitrogen Dewar similar to that used in other infrared focal plane array testing.[20] The device was mounted at 45° from the proton beam direction and held at 80K during the test. The dark- and photo-currents were measured as a function of the APD bias voltage (i.e. I-V curves) using a picoampere meter. A blackbody radiation source and a narrow bandpass filter was used as the light source. For the responsivity measurement, a mechanical chopper was used to modulate the light source and a low noise transimpedance amplifier was used to measure the difference in the detector output with and without the light source being blocked by the chopper.

The proton energy on the detector was set to 63 MeV. The proton beam cross section was 70 mm in diameter, which was much larger than the size of the detector. The proton flux during the irradiation was about $4x10^7$ particles/s/cm^2 (8.3 rad(Si)/s). The HgCdTe APD array was grounded but not biased during the proton irradiation. The device was irradiated in several incremental steps to achieve equivalent accumulated doses of 1, 2, 5, 10, 20, 30, 50, and 100 krad(Si), where 1.0 krad(Si) is equivalent to $7.5x10^9$ particles/cm^2 fluence on the HgCdTe APD array. A full device characterization was performed over a range of APD bias voltages before and after each dose of the proton irradiation. A final measurement was performed after warming the device to room temperature overnight and cooled down again to 80K.

The test devices were selected from the same batch as the devices DRS developed for NASA GSFC. The particular device for this test had a Cu and Hg-vacancy doping, which had smaller p-n junction diameter and higher gain than the Hg-vacancy doped devices. The measurements were automated to measure the I-V curves of 4 of the 16 pixels, which had the lowest initial dark currents (<0.5 pA gain normalized dark current). The device was fully characterized at DRS prior to the proton irradiation test at CNL. The device was also characterized, annealed, and re-characterized back at DRS after the test at CNL.

3.2 Test results of the 4x4 HgCdTe APD array without ROIC

The dark currents from the four pixels vs. APD bias voltage were measured before irradiation and at all intermediate steps. The Dewar leakage current was in the order of 0.3 pA and became negligible compared to the dark current when the APD was biased >10 V. Figure 2 shows the results from one of the pixel with the APD biased at 12 V (gain>1000). It shows the dark current increased roughly linearly with the proton fluence by more than 100 time at 100 krad(Si). All four pixels showed similar behavior with the rate of the dark current increase varying from $2.8x10^{-22}$ to $1.3x10^{-21}$ A/protons/cm^2 from pixel to pixel. The median value was $8.58x10^{-22}$ A/protons/cm^2.

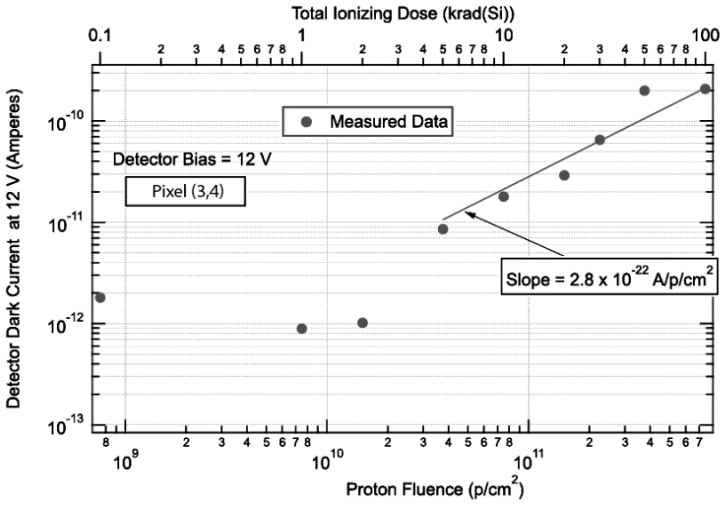

Figure 2. Dark current vs. proton fluence of the HgCdTe APD, Pixel (3,4), at 12 V APD bias.

The devices exhibited an unexpected anti-annealing behavior. The dark currents at 12 V APD bias increased by more than 100 times after warming up to room temperature and cooled down again. All the four pixels measured had similar behavior. The dark currents remained nearly unchanged after storing the device at room temperature for 8 weeks using the same test setup by IRREL/AFRL. The device was sent back to DRS. The APD dark currents were measured again using the DRS test setup which confirmed the IRREL/AFRL measurement results. The device was then baked out at 100°C for 72 hours. The dark currents of the four pixels which we monitored at CNL returned to the pre-irradiation levels. We found that the dark currents of all but one of the 16 pixels on annealed out after the bake out, with most of them returning to their pre-irradiation levels.

There appeared to be a slight degradation (<6%) in the photon-to-electron conversion efficiency under a fixed illumination level at APD biases of 0.05, 1, 3, and 5 V. Figure 3 shows the measurements from one pixel. All four pixels showed similar behavior. The APD gain and quantum efficiency were measured again back at DRS prior to the high temperature bake out. The results were compared with those from a control device on the same wafer. The APD gain and quantum efficiency were found unchanged within the measurement uncertainty. It was possible that the small degradation in the photon-to-electron conversion efficiency observed by IRREL/AFRL during the test at CNL were annealed over the 2-3 months period after proton irradiation when DRS characterized the device.

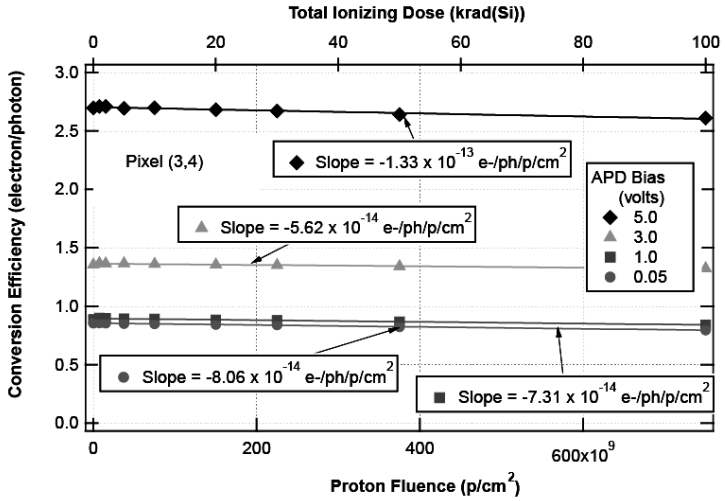

Figure 3. Photon-to-electron conversion efficiency vs. proton fluence of the HgCdTe APD, Pixel (3,4), at several APD bias.

4. PROTON IRRADIATION OF 4X4 PIXEL HGCDTE APD ARRAY WITH ROIC

4.1 Test setup

During the week of 16 September 2013 a second proton radiation damage test was performed to the same 4x4 pixel HgCdTe APD array with the ROIC The test was conducted at the same test facility as the first test and used same test Dewar system but different data acquisition system. The device being tested had a Hg-vacancy doping. It was fully characterized at DRS before being delivered to IRREL/AFRL. With the presence of the ROIC, the APD currents were not directly measurable, as in the case of the fanout array. Instead, the outputs of the ROIC in its capacitive transimpedance preamplifier (CTIA) mode were used to measure the APD current. The outputs of the ROIC in resistive transimpedance amplifier (RTIA) mode were also monitored, though it was not sensitive enough to resolve changes in the APD output due to proton irradiation. The device was re-tested, annealed, and re-characterized back at DRS after the proton irradiation at CNL.

The average proton flux was about 8.8×10^7 particles/s/cm^2 (16.5 rad(Si)/s). The HgCdTe APD array was grounded but not biased during the proton irradiation. The device was irradiated up to 30 krad(Si) in several steps. A low proton flux test was also performed with the device fully powered and the APD biased to near its maximum gain. The proton flux was monitored to be 1300-13,000 particles/s, which was comparable to the maximum flux the detector would experience in a near Earth orbit.

4.2 Test results of the 4x4 HgCdTe APD array with ROIC

The APD dark currents were inferred from ROIC CTIA outputs in this case. The CTIA gain was calibrated before the test and it was found to be 2.4 μV/electron, which was close to the designed feedback capacitance of the CTIA (63 pF, or 2.5 μV/electron)[13]. The output noise was about 0.25 mV, that corresponded 100 electrons, or about 0.01 pA APD current over the 1 ms integration time. The noise was further reduced by averaging a number of CTIA outputs. The ROIC operated in an integration and dump mode with a maximum output voltage was 2.0 V, which gave a linear dynamic range of 800,000 electrons over 1 ms (0.13 nA).

They APD dark currents from five pixels were measured at an APD bias of 10V up to 30 krad(Si). The dark currents rose linearly with proton fluence, similar to those shown in Fig. 2, but at rates ranging from $1x10^{-22}$ to $7x10^{-22}$ A/proton/cm^2. The median value was $4.4x10^{-22}$ A/protons/cm^2. The rate of dark current increase would be 4 times higher at 12 V APD bias voltage, or $1.8x10^{-21}$ A/protons/cm^2, which was roughly two times the rate measured during the first proton test with a similar HgCdTe APD array but without the ROIC.

The dark currents from these five pixels all increased by more than a factor of 10 and well beyond the linear dynamic range of the CTIA after warming up overnight and cooling down again. This confirmed the "anti-annealing" effects seen in the first proton test. The test device was sent back to DRS and tested again. The APD dark currents were found to be largely unchanged after a 2.5 months period in storage at room temperature. The device was then baked out at 90°C for 72 hours and the dark currents measured again. Figure 4 shows the results. As in the first test, the dark current returned to the pre-irradiation levels.

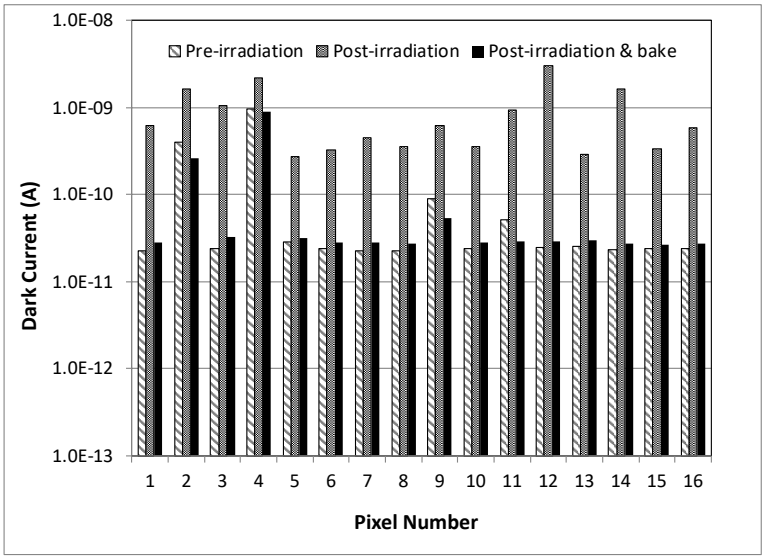

Figure 4. Dark currents of the HgCdTe APD before and after a 30 rad(Si) proton irradiation. The dark currents returned to the pre-irradiation levels after a 72-hour 90°C bake out.

The APD responsivity was also monitored after each proton dose at CNL using a blackbody source at 0.05, 1.0, 2.5, 5.0, 7.5, and 10 V APD bias. Figure 5 shows the median measurement results at 0.05 and 10 V APD bias. The responsivity at 0.05 V APD bias gave a measure of the quantum efficiency since the APD gain at such a low bias level could be assumed as unity.[13] The results at 10 V APD bias gave a measure of the product of the quantum efficiency, the APD gain, and the CTIA gain. These results showed the quantum efficiency decreased linearly with proton doses, by 18% at 30 krad(Si). The responsivity of the device at 10 V APD bias decreased by more than a factor of two but largely annealed after warming up to room temperature overnight. After factoring out the 18% change in the quantum efficiency, the product of the APD gain and CTIA gain was nearly unchanged after annealing.

The post irradiation testing back at DRS showed that the quantum efficiency annealed and almost returned to the original level after a 2.5-month storage at room temperature. Baking the device at 90°C for 72 hours completely restored the quantum efficiency and gain back to the pre-irradiation levels.

Comparing results from the first proton irradiation testing, it was possible that the changes ascribed to the HgCdTe APD quantum efficiency were caused by the ROIC. The CTIA gain was determined by the feedback capacitance, which could vary due to ionization of the insulation layer by the protons. The APD dark currents, on the other hand, increased linearly with proton fluence during both tests and jumped up by 10 to 100 times after the devices were warmed up to room temperature. The increase in the dark currents in the second test was probably as large as that from the first test but were obscured by the CTIA saturation.

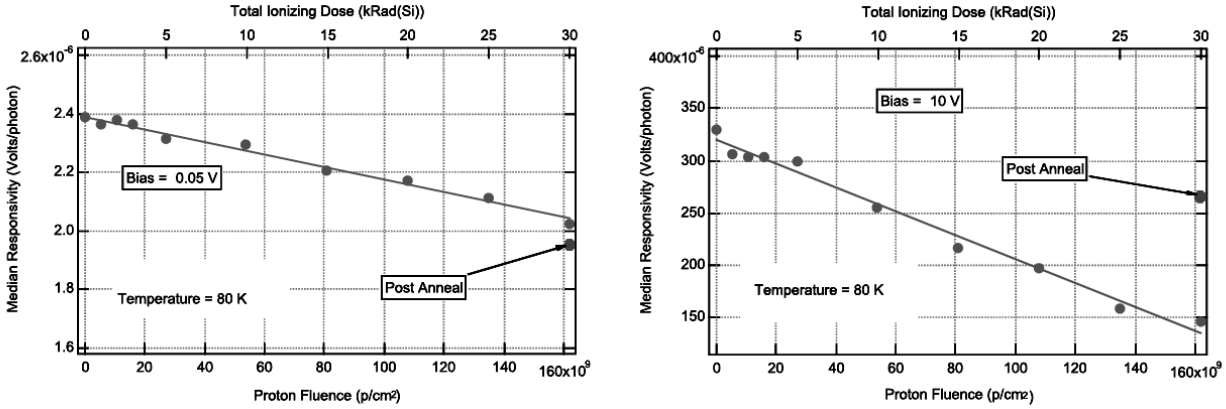

Figure 5. HgCdTe APD median responsivity vs. proton dose up to 30 rad(Si) at 0.05 V APD bias (left) and 10 V bias (right).

The ROIC RTIA output noise levels were measured at each proton dose steps and no changes were observed. The APD bias was set to 0.05V in these measurements so that there was no contribution from the APD noise.

The RTIA output noise levels were re-measured at DRS 2.5 months after the proton irradiation at 0.5 and 10 V APD bias. The noise measured at 0.5 V APD bias were similar to similar to those measured at CNL and unchanged from the pre-irradiation level. The noise measured at 10 V APD bias showed the effect of the APD dark currents. Figure 6 shows the noise equivalent power (NEP) obtained by dividing the pixel output noise by the responsivity. The NEP from each pixel roughly followed the dark current shown in Fig. 4.

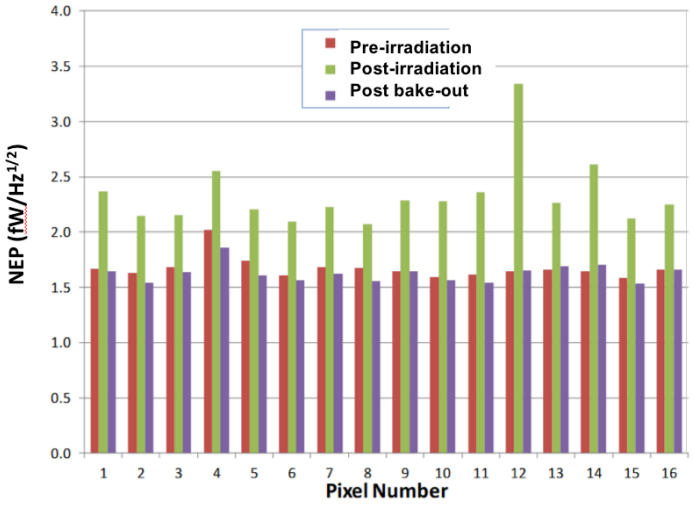

Figure 6. NEPs of the HgCdTe APD before and after a 30 rad(Si) proton irradiation. The NEPs returned to the pre-irradiation levels after a 72-hour 90°C bake out.

A bare ROIC chip was also irradiated separately to 100 krad(Si) with all the input and output terminals grounded and it was held at room temperature. The ROIC chip was sent back to the supplier, ADIC Inc. and re-characterized two months after the irradiation. All ROIC parameters were unchanged to within the uncertainty of the measurement.

The transient response of the device was also measured with the device powered on at 10 V APD bias (APD gain about 300) and a proton flux that each pixel received a photon once a few seconds. The ROIC was operated in CTIA mode. The results showed that the APD produced a large current pulse for each proton hit, with most saturating the CTIA output (800,000 electrons). Dividing by the APD gain (200), each proton on average created an impulse of >40,000 electrons. The results also showed that the ROIC was often overloaded by the large current pulses and latched up at the maximum output until the APD bias was lowered to below 3 V. We later reproduced the latch up state with relatively strong laser pulse. We believed this was caused by a voltage clamping diode in the ROIC, which could be fixed in another design iteration.

5. GAMMA RAY IRRADIATION OF 4X4 HGCDTE APD ARRAY WITHOUT ROIC

5.1 Test setup

The gamma-ray radiation exposure test was performed using the ^{66}Co test source at NASA GSFC on 21 October 2015. Gamma ray caused only ionization damage and the results could be used to better understand the results from protons that caused both ionization damage and displacement damage. Only the APD dark currents were measured since they were the primary radiation damage effects based on our test results from the proton tests.

The test device was a bare 4x4 pixel HgCdTe APD array without ROIC. The device was housed inside a generic liquid nitrogen Dewar and held at 80K during the irradiation and intermediate and post irradiation characterization. The Dewar window and the cold filter were replaced with aluminum blanks to ensure that no optical or thermal photons were illuminating the detector. The five pixels with the lowest initial dark currents were selected and wired out for measurement. The APD currents were measured as a function of the bias voltage (I-V curves) by using a picoampere meter. In this test the leakage currents were much higher than that for the earlier proton tests, but still below the dark current of the HgCdTe APDs when biased above 7 V.

The radiation dose rate was set to 10 rad(Si)/s, which was comparable to that during the proton irradiation tests. The dose rate was verified by placing a dosimeter in the Dewar at the same position of the detector with Dewar cover in place during the test setup. The device was irradiated in step to 2, 5, 10, 20, 30, 50, and 100 krad(Si). The detector was grounded but not biased during the irradiation. The I-V curves were measured after each step of exposure. Post irradiation measurements were performed at GSFC and then at DRS.

5.2 Test results of the gamma ray irradiation of the 4x4 HgCdTe APD array without ROIC

The APD dark currents showed no measurable change with gamma ray irradiation up to 100 krad(Si). There was some increase in the measured dark currents but we could not positively identify if that was from the device or the Dewar system. The device was sent back to DRS and the APD currents were re-measured using their low background leakage current test setup. There were no changes observed when compared to pre-irradiation measurement results. Therefore, the device appeared not susceptible to gamma ray irradiation up to 100 krad(Si). The radiation damage observed from the proton tests were likely displacement damage.

6. PROTON IRRADIATION OF 2X8 PIXEL HGCDTE APD ARRAYS WITH ROIC

6.1 Test setup

Another proton radiation exposure was performed with the 2x8 pixel HgCdTe APD arrays and the built-in ROIC. The major objectives were to investigate the transient effects, the annealing behavior, and annealing techniques. The test was performed at CNL, Davis, CA, during the week of 28 August to 1 September 2017. The APD arrays were housed in the same liquid nitrogen Dewar described above and used an aluminum blank in place of the cold filter. The detectors were held at 80K during the irradiation and intermediate testing. The data acquisition system consisted of an oscilloscope, which recorded the pulse waveforms output from the detector under proton irradiation; and a universal counter that measured the detector dark count rate from each pixel as a function of the threshold.

Two devices were tested, one with Hg-vacancy doping and one with Cu and Hg-vacancy doping. As mentioned earlier, these 2x8 pixel devices were similar to the 4x4 pixel devices, with the HgCdTe material from the same batch and the ROICs made by the same process at the same foundry service. The general findings from the tests should be common to both types of the devices.

The proton energy after the Dewar window and the aluminum blank on the detectors was about 55.4 MeV. The proton flux was first set to about 10^5 particles/s/cm^2 that each pixel was hit by individual protons several times a second and the detector response to each proton could be recorded. For this test the detectors were fully powered. The proton flux was then increased to about 2.5×10^7 for accumulated dose tests with the devices powered off. The detector dark count rates were measured after 2, 5, and 10 krad(Si) steps. The devices were warmed up to room temperature overnight and cooled to 80K again the next day to assess their annealing behavior. The devices were then heated to different temperatures for different durations and cooled again to see the annealing effects. An effective annealing process was determined through these repeated heating cycles. One of the devices was irradiated again by another 10 krad(Si) while powered on after it was totally annealed from the first 10 krad(Si) dose. The devices were heated to the optimal annealing temperature and cooled down several times to compare annealing rate after the 20 krad(Si) total accumulated dose.

6.2 Transient effects of proton bombardment

The detector outputs were monitored while being irradiated by protons at a low flux. The APD bias was first set to 0 V (unity gain). There were large current pulses output from each pixel at rate corresponding to the proton hit rate per pixel. The APD bias was then increased to 4, 8, 11, and 12 V. Figure 7 shows sample pulse waveforms from the detector with a ½ losses due to a power splitter. The output of the APD at 0 V bias was largely unsaturated and could be used to estimate the electrons generated by each proton. Since the average pulse amplitude for a single photon at an APD gain of 1000 was about 7 mV, the maximum unsaturated pulse waveforms shown in Fig. 7 corresponded to about 100,000 electrons/proton. At higher APD bias, the detector outputs were mostly saturated but recovered by themselves. A long appeared after each pulse, but they completely returned to the original level well within 5 μs. The detector was bombarded at this proton flux for about an hour and there was no sign of degradation. All pixels functioned nominally. There were sometimes glitches in the waveforms when adjacent pixels were hit by protons. Occasionally the dark count rates from a pixel could go up for a period of time before returned to the original level. There was no latch-up after overload from this ROIC. Both devices tested showed the same behavior.

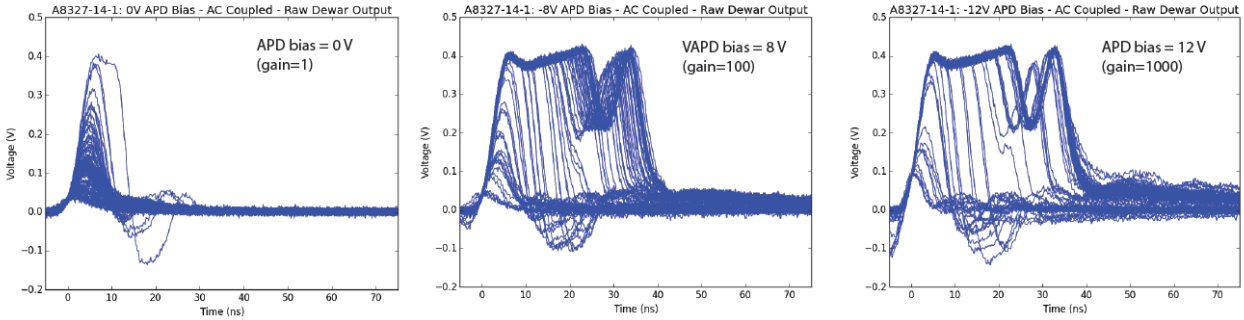

Figure 7. Sample HgCdTe APD output pulse waveforms in response to proton hits with the APD biased at 0, 8, and 12 V.

6.3 Annealing of the proton radiation damage

The devices were then irradiated to 10 krad(Si) and their annealing behaviors were monitored through a series of high temperature bakes of short duration. From the previous tests, the dark currents increased significantly after warming up to room temperature but returned to normal after an extended high temperature bake. The objective of this test was to find the lowest temperature and shortest duration for the device to anneal.

It was found that the devices started to show radiation damage at 10 krad(Si) and warming up the devices to room temperature overnight caused the dark count rates to increase significantly, just like in the previous two proton tests. Baking the devices at 70°C had little effect. However, baking at 85°C for 3-4 hours reduced the dark count rates from

proton irradiation back to the original levels for both of the devices. Figure 8 shows the dark count rates vs. threshold voltage for the Hg-vacancy doped devices before and after the proton irradiation and after a 3-hour 85°C bake. It shows the radiation damage were isolated to a few pixels up to 10 krad(Si) while the devices were kept at 80K, but damage expanded to all pixels after warming up to room temperature. The damage largely disappeared after baking the device to 85°C for 3 hours.

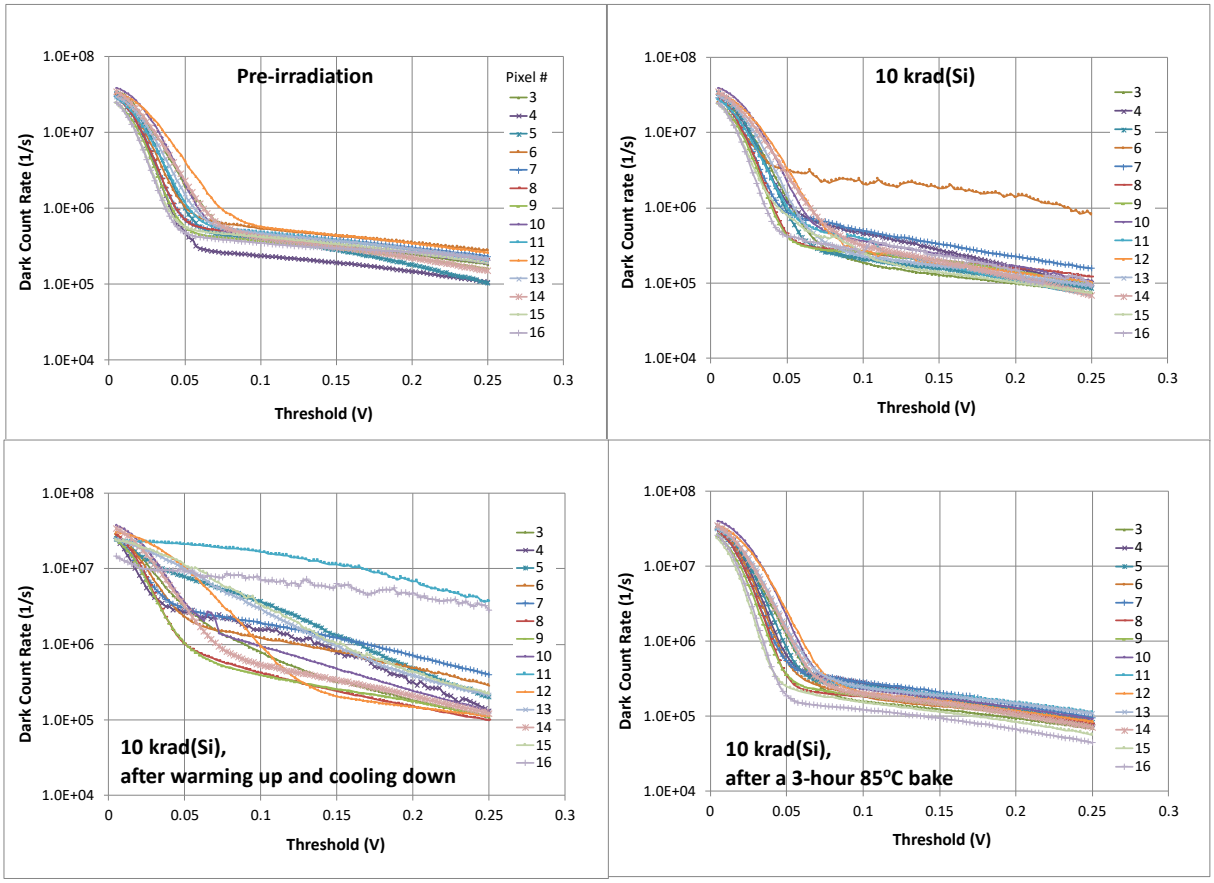

Figure 8. HgCdTe APD dark count rates vs. threshold before proton irradiation (top left), after 10 krad(Si) proton irradiation, after warming up to room temperature overnight, and after a 3-hour 85°C bake. The data were from the Hg-vacancy doped devices, though the Cu-Hg doped device showed similar behavior. The measurements were taken with a universal counter with the device at 80K.

The Hg-vacancy doped device was irradiated again by another 10 krad(Si) protons (total 20 krad(Si)) after it was fully annealed through 4.5 hours 85°C bake. The dark count rate vs. threshold was measured at GSFC after a series of heating cycles back to confirm the annealing technique. The results are shown in Fig. 9. The detector's annealing behavior was similar to that after the first 10 krad(Si) proton irradiation. Baking at 70°C was found ineffective. The dark count rate did not completely return to the original level after the first 85°C bake but eventually did after a total of 12 hours 85°C bake.

We also measured the APD responsivity in (V/W) and the APD gain using a pulsed laser before the proton irradiation and after the last high temperature baking. There were no measurable degradations after the tests.

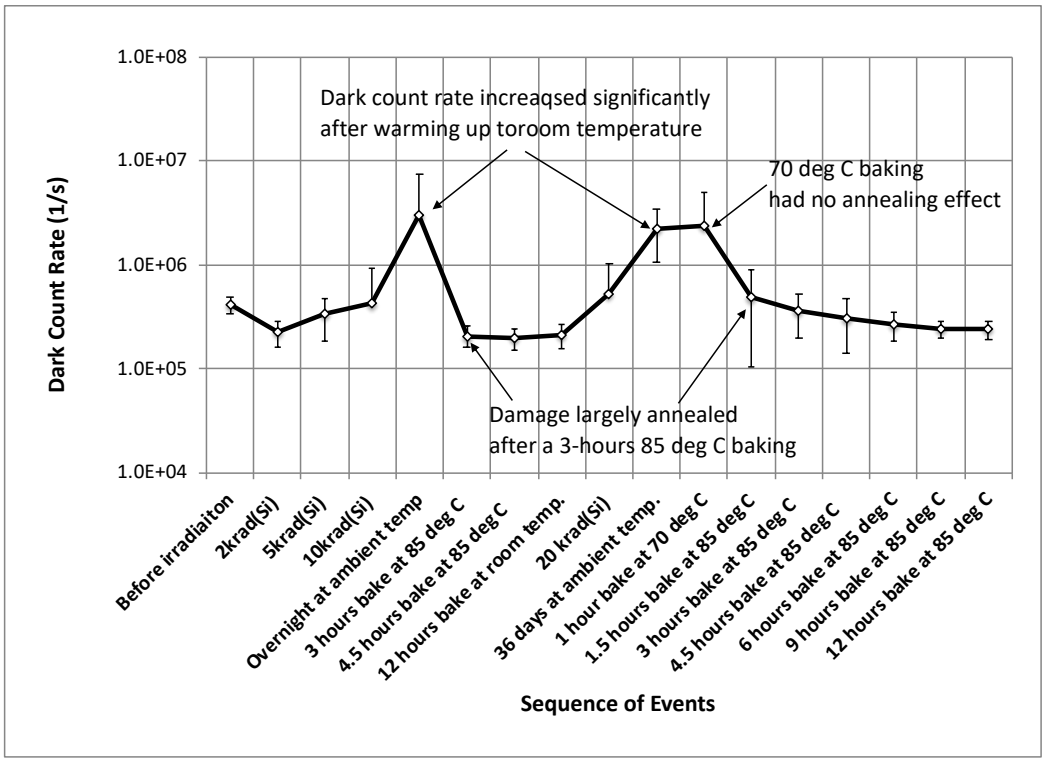

Figure 9. The 2x8 pixel HgCdTe APD dark count rates vs. threshold through the sequence of events of proton irradiation and annealing. The data was from the Hg-vacancy doped device.

7. SPACE APPLICATIONS AND RADIAITON DAMAGE MITEGATION

For a typical low-Earth orbital mission, the primary radiation sources to be considered are solar protons and trapped protons that have energies up to several hundred MeV.[24] There are also trapped electrons with energy up to 5 MeV. Protons and electrons can cause displacement damage as well as ionization damage in detectors.

Detectors used in space lidar receivers are usually well shielded by the optics in front, lens housing on the side, and the electronics on the back. For example, the lidar detectors on the Geoscience Laser Altimeter System (GLAS) on the ICESat mission had an estimated dose of <15 krad(Si) for most of the electronics over 5 years with 2.5 mm aluminum shielding, but <5 krad(Si) for the lidar detectors. The primary type of radiation after the shielding are protons from a few to several hundred MeV at a fluence of about 10^{10} particles/cm^2. The peak flux was estimated to be about 1,000 protons/cm^2/s, or an average of about 0.04 proton hits/s..

The results from proton and gamma ray tests show that these HgCdTe APD arrays can be used in a space lidar in low Earth orbit. There is little permanent damage from ionization. Most of the radiation effects are displacement damage which causes the dark current to rise. The detector quantum efficiency and the APD gain were not seriously affected by radiation. Transient effects from proton hits were seen to produce large pulses that can interrupt normal signal detection, but the pulses only lasted a few microseconds. Persistent radiation damage started to become evident after 5-10 krad(Si) when the detector was kept at the cryogenic temperatures. The APD dark currents due to radiation damage increased significantly after the detector was brought to room temperature. However most of the radiation damage, both the accumulated when the detector was at cryogenic temperature and the newly released damage at room temperature, was annealed by heating the device at 85°C for several hours. Therefore, the radiation damage to these HgCdTe APD arrays was seen to be mitigated by periodically heating the devices.

8. CONCLUSIONS

A series radiation damage tests were performed on HDVIP® HgCdTe APD detector arrays that were fabricated by Leonardo DRS Electro-Optical Infrared Systems. The most significant effect was the increase of the APD dark currents. The detector quantum efficiency and the APD gain decreased only slightly at 100 krad(Si). The detectors also produced a large current impulse in response to each proton hit, but the response completely recovered within 1 μs. The increased dark current caused radiation damage was found to increased significantly after the devices were brought to room temperature. However almost all of the radiation damage was found to anneal after heating the device to 85°C for several hours, which can be used as a mitigation technique. The devices appear well suited for use as space lidar detectors if they are annealed periodically.

ACKNOWLEDGEMENTS

We thank NASA Earth Science Technology Office (ESTO) for supporting these radiation tests. We also thank IRREL/AFRL for conducting the first two proton radiation tests. We thank the staff at CNL for arranging the tests and the logistics. We thank Dr. Issak Samsel of NASA GSFC for the support of the third proton radiation test. We thank Mr. James McCurdy of DRS for preparing the test samples and the test setups.

REFERENCES

[1] Waczynski, A, Beck, T., Boucarut, R., Cheng, E., Cottinghan, D., Delo, G., Fixsen, D., Hill, F. J., Johnson, S., Kenny, P., Landsman, W., Malumuth, E., Offenbert, J., Polidan, E., Russell, A. M., Schlossbert, D., Sharp, E., Wassell, E., Wen, Y., and Yagelowich, J., "HgCdTe detectors for the Hubble Space Telescope Wide Field Camera 3 IR Channel," in [Scientific Detectors for Astronomy] 300, 175-182 Springer, Dordrecht (2004).

[2] Rauscher, B. J., Boehm, N. Cagiano, S., Delo, G. S., Foltz, R., Greenhouse, M. A., Hickey, M., Hill, R. J., Kan, E., Lindler, D., Mott, D. B., Waczynski, A., and Wen, Y., "New and better detectors for the JWST near-infrared spectrograph," Astronomical Society of the Pacific, 126, 739-749 (2014).

[3] James Webb Space Telescope, "Infrared Detectors," <https://jwst.nasa.gov/infrared.html>, (21 March 2018).

[4] Beck, J., Wan, C., Kinch, M., Robinson, J., Mitra, P., Scritchfield, R., Ma, F., and Campbell, J., "The HgCdTe electron avalanche photodiode," J. Electron. Mater. 35(6), 1166-1173 (2006).

[5] Kinch, M. A., [Fundamental of Infrared Detector Materials], SPIE Press, Bellingham, ch. 7 (2007).

[6] Kinch, M. A., [State-of-the-Art Infrared Detector Technology], SPIE Press, Bellingham, ch. 6 (2014).

[7] Baker, I. and Kinch, M, "HgCdTe electron avalanche photodiodes (EAPDs)," in [Mercury Cadmium Telluride: Growth, Properties and Applications], Capper, P. and Garland, J. ed. (John Wiley & Sons, Chichester, ch. 21 (2011).

[8] Baker, I. M., Maxey, C., Hipwood, Les, and Barnes, K., "Leonardo (formerly Selex ES) infrared sensors for astronomy – present and future," Proc. SPIE 9915, 991505 (2016).

[9] Rothman, J., Mollard, L., Gout, S., and Wlassow, J., "History dependent impact ionization theories applied to HgCdTe e-APDs," J. Electron. Mater. 40(8), 1757–1768 (2011).

[10] Dumas, A., Rothman, J., Gibert, F., Edouart, D., Lasfargues, G., Cenac, C., Mounier, F. L., Pellegrino, J., Zanatta, J. P., Bardoux, A., Tinto, F., and Flamant, P., "Evaluation of a HgCdTe e-APD based detector for 2 μm CO_2 DIAL application," Applied Optics 56(27), 7577-7585 (2017).

[11] Jack, M., Wehner, J., Edwards, J., Chapman, G. Hall D. N. B., and Jacobson, M., "HgCdTe APD-based linear-mode photon counting components and LADAR receivers," Proc. SPIE 8033, 80330M (2011).

[12] Beck, J., Welch, T., Mitra, P., Reiff, K., Sun, X., and Abshire, J. "A highly sensitive multi-element HgCdTe e-APD Detector for IPDA lidar applications," J. Electron. Mater. 43(8), 2970-2977 (2014).

[13] Sun, X, Abshire, J. B., Beck, J. D., Mitra, P., Reiff, K., and Yang, G., "HgCdTe avalanche photodiode detectors for airborne and spaceborne lidar at infrared wavelengths," *Optics Express*, 25(14) 16589-16602 (2017).

[14] Beck, J. D., Scritchfield, R., Mitra, P., Sullivan III, W. W., Gleckler, A. D., Strittmatter, R., and Martin, R. J., "Linear mode photon counting with the noiseless gain HgCdTe e-avalanche photodiode," Opt. Eng. 53(8), 081905 (2014).

[15] Sullivan, W., Beck, J., Scritchfield, R., Skokan, M., MItra, P., Sun, X., Abshire, J. Carpenter, D., and Lane, B., "Linear-mode HgCdTe avalanche photodiodes for photon-counting applications," J. Electron. Mater. 44(9) 3092-3101 (2015).
[16] Marshall, P. W., Hubbs, J. E., Arrington, D. C., Marshall, C. J., Reed, R. A., Gee, G., Pickel, J. C., and Romos, R. A., "Proton-induced transients and charge collection measurements in a LWIR HgCdTe focal plane array," IEEE. Trans. Nuclear Science 50(6), 1968-1973 (2003).
[17] McKelvey, M. E., Ennico, K. A., Johnson, R. R., Marshall, P. W., McMurray Jr., R. E., McCreight, C. R., Pickel, J. C., and Reed, R. A., "Radiation environment performance of JWST prototype FPAs," Proc. SPIE 5167, 223-234 (2004).
[18] Pickel, J. C., Reed, R. A., Ladbury, R., Marshall, P.W., Jordan, T. M., Gee, G., Fodness, B., McKelvey, M., McMurray, R., Ennico, K., McGreight, G., Waczynski, A., Polidaan, E. J., Johnson, S. D., Weller, R. A., Mendenhall, M. H., and Schrimpf, R. D., "Transient radiation effects in ultra-low noise HgCdTe IR detector arrays for space-based astronomy, IEEE Trans. Nuclear Science 52(6), 2657-2663 (2005).
[19] Waczynski, A., Marshall, P. W., Marshall, C. J., Foltz, R., Kimble, R. A., Johnson, S. D., Hill, R. J., "Radiation induced luminescence of the CdZnTe substrate in HgCdTe detetors for WFC3," Proc. SPIE 5902, 59020P (2005).
[20] Hubbs, J. E., Marshall, P. W., Marshall, C. J., Gramer, M. E., Maestas, D., Dole, G. A., and Anderson, A. A., "Lateral diffusion length changes in HgCdTe detectors in a proton environment, IEEE Trans. Nuclear Science 54(6) 2435-2443 (2007).
[21] Weber, A., Belzner, W., Haas, L. D., Hanna, S., Hofmann, K., Neef, A., Reder, M., Stifer, P., Wendler, J., Ziegler, J., Nothaft, H. P., "Radiation hardness of two dimensional focal plane detector arrays for LWIR/VLWIR space sounding missions, Proc. IEEE 12th European Conference on Radiation and its Effects on Components and Systems (RADECS), 336-339 (2011).
[22] Bergeson, J. D., Bommena, R., Fahey, S., Cowan, V., Morath, C., and Velicu, S., "Mid and long wavelength infrared HgCdTe photodiodectors exposed to proton irradiation," Proc. SPIE 9226, 92260P (2014).
[23] Dorn, M. L., Pipher, J. L., McMurtry, C., Hartman, S., Mainzer, A., McKelvey, M., McMurray, R., Chevara, D., and Rosser, J., "Proton irradiation results for long-wave HgCdTe infrared detector arrays for NEOCam," J. Astron. Telsc. Instrum. Syst. 2(3), 036002 (2016).
[24] Stassinopoulos, E. G., and Raymond, J. P., "The space radiation environment for electronics," Proc. IEEE 76(11) 1423-1442 (1988).